

Analytical Expression for Fracture Profile in Viscoelastic Crack Propagation

Hokuto Nagatakiya,¹ Naoyuki Sakumichi,^{2,*} Shunsuke Kobayashi,¹ and Ryuichi Tarumi^{1,†}

¹Graduate School of Engineering Science, Osaka University,
1-3 Machikaneyama, Toyonaka, Osaka 560-8531, Japan

²Department of Chemistry and Biotechnology, The University of Tokyo, Bunkyo-ku, Tokyo 113-8656, Japan
(Dated: December 14, 2023)

We derive an analytical expression for the strain field, including fracture profile, during steady-state crack propagation in viscoelastic solids. This expression, featuring the hypergeometric function, is obtained by exactly solving a model that incorporates the standard linear solid (i.e., three-element Zener) model. We find three regions in the fracture profile, distinguished by power-law exponents that evolve with distance from the crack tip; this explains why crack tips become sharper in rubbers and gels as the crack-propagation velocity increases. We also provide a solid foundation for de Gennes' viscoelastic trumpet, previously based only on a scaling argument. These insights should help prevent catastrophic failure of polymer materials triggered by velocity jumps.

Viscoelastic soft materials, such as rubbers and gels, find application in diverse industrial contexts, medical instruments, and even within the realm of food products. Understanding their fracture characteristics [1–3] is therefore not only of scientific interest but also of great practical importance. For example, both rubbers [4–10] and gels [11, 12] may fail catastrophically due to abrupt increases in crack-propagation velocity, triggered by a rise in sharpness at the crack tip. This increased sharpness cannot be explained by linear elastic fracture mechanics (LEFM) [13], where the surface of static cracks exhibits a parabolic profile. However, in the case of viscoelastic soft materials such as rubbers [7, 14, 15] and gels [16–20], increased crack velocity leads to a sharper, non-parabolic profile near the crack tip.

The weakly nonlinear theory of dynamic fracture [17], an extension of LEFM that accommodates second-order nonlinearity but omits viscoelasticity, can account for this sharpening in certain experimental settings [7, 16, 18]. Nevertheless, it inadequately explains the sharpening observed in filler-reinforced synthetic rubber, in which cracks propagate rapidly [7]. This highlights the necessity to include viscoelastic properties, which have not yet been fully incorporated into continuum fracture mechanics.

A pioneering fracture theory that incorporates viscoelastic properties is the “viscoelastic trumpet” proposed by de Gennes [21, 22]. For analytical simplicity, this theory adopts a standard linear solid model in which the dependence of the complex modulus μ on frequency ω is given by

$$\mu(\omega) = \mu_0 + (\mu_\infty - \mu_0) \frac{i\omega\tau}{1 + i\omega\tau}. \quad (1)$$

This model is characterized by the relaxation time τ and low- and high-frequency elastic moduli μ_0 and μ_∞ , respectively, with the ratio $\lambda \equiv \mu_\infty/\mu_0 \sim 10^2\text{--}10^3$ [21–24]. Instead of taking the traditional fracture-mechanics

approach that directly addresses continuum mechanics problems, de Gennes applied scaling analysis combined with energy balance. Through this scaling analysis, he predicted that the fracture profile would be divided into three separate regions, each distinguished by characteristic power-law exponents; the overall fracture profile conjectured to be trumpet-shaped. However, in the absence of direct solutions in continuum mechanics, it has remained unclear how the viscoelastic trumpet is related to traditional fracture mechanics. Efforts to validate the theory, whether by finite element methods (FEM) or by experiments [25, 26], have been limited, leaving a decisive confirmation unresolved.

In this Letter, we investigate how viscoelastic properties lead to progressive sharpening of the crack tip as the crack-propagation velocity increases. Focusing on steady-state crack propagation in linear viscoelastic solids, we adopt the complex modulus given by Eq. (1), as employed in the viscoelastic trumpet model. We use the traditional fracture mechanics approach, which seeks to explain all observed phenomena directly from the first principles of continuum mechanics. However, following de Gennes, we simplify the problem by introducing certain assumptions that have a negligible influence on the fracture profile. Adopting these assumptions, we successfully derive an analytical expression for the strain field, including the fracture profile. From this expression, we identify three distinct regions within the fracture profile, each characterized by a different power-law exponent depending on the distance from the crack tip. Notably, these exponents are consistent with those of the viscoelastic trumpet. Our analytical results validate the viscoelastic trumpet and elucidate its position in continuum fracture mechanics. They also illuminate the origin of crack-tip sharpening, which prior studies [7, 16–18] attributed to the nonlinear stress-strain relationship; our analysis reveals that even in the linear elastic regime, viscoelasticity can amplify sharpening at elevated crack-propagation velocities.

Setup.— As shown in Fig. 1(a), we consider a two-dimensional viscoelastic sheet of height $2L$ and infinite

* Corresponding author: sakumichi@gel.t.u-tokyo.ac.jp

† Corresponding author: tarumi.ryuichi.es@osaka-u.ac.jp

width with a semi-infinite linear crack at its center. In its undeformed state, the crack aligns with the x -axis. The sheet is subjected to a strain ε induced by a fixed boundary condition. This applied strain causes the crack to propagate in the $-x$ direction at a constant velocity V . Focusing on steady-state crack propagation, all fields at position (x, y) and time t are represented as functions of $(x + Vt, y)$. Thus, without loss of generality, we can analyze the displacement field at time $t = 0$ when the crack tip is located at $x = 0$. The fixed boundary and stress-free boundary conditions for this setup are as follows [27, 28]:

$$\begin{cases} u_x(x, \pm L) = 0 & (\text{for } -\infty < x < \infty) \\ u_y(x, \pm L) = \pm \varepsilon L & (\text{for } -\infty < x < \infty) \\ \sigma_{xy}(x, \pm 0) = \sigma_{yy}(x, \pm 0) = 0 & (\text{for } 0 < x < \infty), \end{cases} \quad (2)$$

where $u_i = u_i(x, y)$ is the displacement field, and $\sigma_{ij} = \sigma_{ij}(x, y)$ ($i, j = x, y$) is the Cauchy stress tensor. The coordinates $(x, \pm 0)$ for $x > 0$ correspond to the upper and lower surfaces of the crack, respectively.

Our main objective is to determine the fracture profile (i.e., the displacement fields on the crack surface) $\mathcal{U}(x) \equiv u_y(x, +0)$ for $x > 0$ assuming the x -axis symmetry: $u_y(x, +0) = -u_y(x, -0)$. According to Okumura and de Gennes [29], $u_x(x, y)$ is approximately zero within this sheet and therefore has only a minor influence on the fracture profile $\mathcal{U}(x)$. Thus, in this study, we assume

$$u_x(x, y) = 0, \quad (3)$$

for $-\infty < x < \infty$ and $-L \leq y \leq L$.

In continuum mechanics, the law of motion is described by the momentum balance equation [13]:

$$0 = \sum_{j=x,y} \partial_j \sigma_{ji} \quad (\text{for } i = x, y). \quad (4)$$

Here, we omit the inertial term to clarify the relationship between fracture profile and linear viscoelasticity. This simplification is justified when the crack-propagation velocity V is significantly lower than the shear wave velocity [8, 21].

We employ the Zener model [30], shown in Fig. 1(b), to give the relationship between the Cauchy stress σ_{ij} and Cauchy strain $\mathcal{E}_{ij} \equiv (\partial_i u_j + \partial_j u_i)/2$. Assuming a zero Poisson ratio, the viscoelastic stress-strain relationship of the Zener model with plane-stress conditions is as follows:

$$\sigma_{ij} \equiv 2\mu_0 \mathcal{E}_{ij} + \sigma_{ij}^{\text{vis}}, \quad (5)$$

$$\sigma_{ij}^{\text{vis}} \equiv 2\eta \partial_t \mathcal{E}_{ij}^{\text{vis}} = 2\mu_1 (\mathcal{E}_{ij} - \mathcal{E}_{ij}^{\text{vis}}), \quad (6)$$

where σ_{ij}^{vis} and $\mathcal{E}_{ij}^{\text{vis}}$ are the Cauchy stress and strain in the dashpot, respectively. As shown in Fig. 1(c), the complex modulus $\mu(\omega)$ of the Zener model, given in Eq. (1), captures the three types of dynamic response of viscoelastic solids: soft solid, liquid, and hard solid [21, 22]. Since

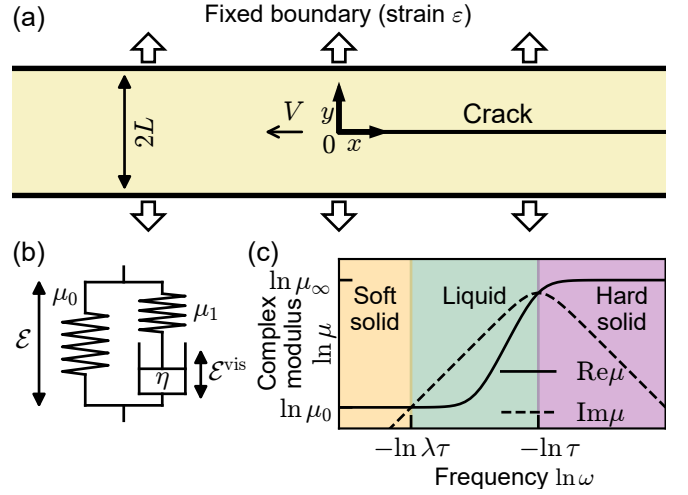


FIG. 1. Setup of viscoelastic crack propagation. (a) Two-dimensional viscoelastic sheet with a semi-infinite linear crack at its center, subjected to a strain ε due to a fixed boundary condition. The crack propagates at a constant velocity V in the $-x$ direction. (b) Zener model: two strings with shear moduli μ_0 and $\mu_1 = \mu_\infty - \mu_0$, interconnected with a dashpot with viscosity η . The strains of the left spring and dashpot are \mathcal{E}_{ij} and $\mathcal{E}_{ij}^{\text{vis}}$, respectively. (c) Complex modulus $\mu(\omega)$ of the Zener model [Eq. (1)] characterizes three types of dynamic response. The relaxation times are $\tau \equiv \eta/\mu_1$ and $\lambda\tau$, where $\lambda \equiv \mu_\infty/\mu_0$.

all fields are functions of $(x + Vt, y)$ in steady-state crack propagation, it follows that $\partial_t = V\partial_x$ [17]. In particular, we have

$$\partial_t \mathcal{E}_{ij}^{\text{vis}} = V \partial_x \mathcal{E}_{ij}^{\text{vis}}. \quad (7)$$

Analytical solution for steady-state crack propagation.— In the setup described by Eqs. (2)–(7), we obtain the analytical solution $u_y = u_y(x, y)$ for steady-state crack-propagation with propagation velocity V . This is achieved through a variable transformation that reformulates the viscoelastic steady-state crack propagation problem into an equivalent static-crack problem where the crack does not propagate. Accordingly, the corresponding static crack solution $u_y^0 = u_y^0(x, y)$ is required. In a static-crack problem, Eqs. (5) and (6) simplify to $\sigma_{ij} = 2\mu_0 \mathcal{E}_{ij}$ because $\sigma_{ij}^{\text{vis}} \equiv 2\eta \partial_t \mathcal{E}_{ij}^{\text{vis}} = 0$. This static-crack problem has been solved by Okumura and de Gennes [29] as follows:

Lemma. (Static crack) Given the boundary conditions in Eq. (2) with Eq. (3), the displacement field satisfying $\sigma_{ij} = 2\mu_0 \mathcal{E}_{ij}$ is given by $u_y(x, y) = u_y^0(x, y)$, where

$$u_y^0(x, y) \equiv \frac{2\varepsilon L}{\pi} \text{Im} \left[\ln \left(e^{-\pi z^*/2L} + \sqrt{e^{-\pi z^*/L} - 1} \right) \right]. \quad (8)$$

Here, $z^* = \sqrt{2}x - iy$ is the complex conjugate of $z = \sqrt{2}x + iy$. In Eq. (8), the branch of the logarithmic function is selected so that $\log z$ has a zero argument for real positive z , and the square root is defined such that $z^{1/2} = i$ for $z = -1$.

Employing the static crack solution in Eq. (8), we obtain the solution for steady-state crack propagation as follows:

Theorem. (Steady-state crack propagation) Given the boundary conditions in Eq. (2) with Eq. (3), the displacement field satisfying Eqs. (4)–(7) is given by

$$u_y(x, y) = u_y^0(x, y) - \left(1 - \frac{1}{\lambda}\right) \times \int_{-\infty}^x \frac{\partial u_y^0(\xi, y)}{\partial \xi} \exp\left(-\frac{x-\xi}{\lambda V \tau}\right) d\xi, \quad (9)$$

where $\lambda \equiv \mu_\infty/\mu_0$ and $\tau \equiv \eta/\mu_1$. Here, $u_y^0(x, y)$ is given by Eq. (8).

As $V \rightarrow 0$, the integrand in Eq. (9) vanishes, resulting in $u_y(x, y)$ converging to $u_y^0(x, y)$ in Eq. (8).

Proof of Theorem. We introduce a transformation relating the intended displacement field $u_i(x, y)$ to an auxiliary field $u_i^0(x, y)$ (for $i = x, y$), defined by

$$u_i^0(x, y) \equiv (1 + \lambda V \tau \partial_x) u_i^{\text{vis}}(x, y), \quad (10)$$

$$u_i^{\text{vis}}(x, y) \equiv \frac{1}{\tau V} \int_{-\infty}^x u_i(\xi, y) e^{-(x-\xi)/\tau V} d\xi. \quad (11)$$

Equation (11) implies $u_i(x, y) = (1 + V \tau \partial_x) u_i^{\text{vis}}(x, y)$. First, we show that $u_i^0(x, y)$ satisfies both the balance equation [Eq. (4)] and the boundary conditions in the static crack. The stress–strain relationship in the static crack is

$$\sigma_{ij} = 2\mu_0 \mathcal{E}_{ij}^0, \quad (12)$$

where we define $\mathcal{E}_{ij}^0 \equiv (\partial_j u_i^0 + \partial_i u_j^0)/2$. Substituting Eq. (7) into Eq. (6), we obtain $\mathcal{E}_{ij} = (1 + V \tau \partial_x) \mathcal{E}_{ij}^{\text{vis}}$. Combining this relationship with Eq. (11), we obtain $\mathcal{E}_{ij}^{\text{vis}} = (\partial_j u_i^{\text{vis}} + \partial_i u_j^{\text{vis}})/2$. Substituting Eqs. (6) and (7) into Eq. (5), we obtain $\sigma_{ij} = 2\mu_0 (1 + \lambda V \tau \partial_x) \mathcal{E}_{ij}^{\text{vis}}$. Combining this equation with Eq. (10), we obtain Eq. (12). Therefore, $u_i^0(x, y)$ satisfies the balance equation in the static crack, as claimed above.

Applying Eq. (2) to Eqs. (10)–(12), we derive the boundary conditions for u_i^0 as

$$\begin{cases} u_x^0(x, \pm L) = 0 & (\text{for } -\infty < x < \infty) \\ u_y^0(x, \pm L) = \pm \varepsilon L & (\text{for } -\infty < x < \infty). \end{cases} \quad (13)$$

These boundary conditions for u_i^0 are thus the same as those for u_i in Eq. (2); the additional stress conditions are the same as in Eq. (2). Therefore, $u_i^0(x, y)$ is simply the displacement field in the static crack, as described in the Lemma.

Next, we derive $u_y(x, y)$. Using Eqs. (3), (10), and (11), we obtain $u_x^0(x, y) = 0$. Substituting Eq. (12) into Eq. (4), we obtain

$$(\partial_x^2 + 2\partial_y^2) u_y^0 = 0, \quad (14)$$

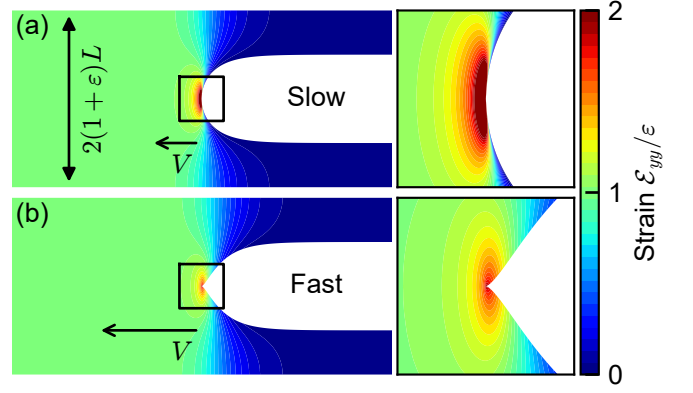


FIG. 2. Strain field \mathcal{E}_{yy} and fracture profile during steady-state crack propagation at a constant velocity V , based on the analytical expression. (a) At low V , the crack-tip profile is approximately parabolic. (b) At high V , the profile deviates significantly from a parabola. Results for other velocities show that the profile grows progressively sharper as V increases.

which has the form of the Laplace equation. The solution of Eq. (14), subject to the boundary conditions [Eq. (13) and the stress conditions in Eq. (2)], is $u_y^0(x, y) = u_y^0(x, y)$, as provided in Eq. (8). To determine $u_y(x, y)$, we employ the variation of constants method. By using Eqs. (8), (10), and (11), we derive $u_y(x, y)$ as given in Eq. (9). Q.E.D.

Analytical expression for fracture profile.— Before investigating the fracture profile $\mathcal{U}(x) \equiv u_y(x, +0) = -u_y(x, -0)$ in steady-state crack propagation as described by Eq. (9), it is instructive to first confirm that the fracture profile $\mathcal{U}^0(x)$ in the static crack solution in Eq. (8) exhibits a parabolic contour near the crack tip. In the limit $y \rightarrow \pm 0$, Eq. (8) yields [29]

$$\mathcal{U}^0(x) = \frac{2\varepsilon L}{\pi} \arctan\left(\sqrt{e^{\sqrt{2\pi x}/L} - 1}\right) \quad (15)$$

for $x > 0$. Introducing the dimensionless coordinate $X = \sqrt{2\pi x}/L$, we deduce that $\mathcal{U}^0(x) = \frac{2\varepsilon L}{\pi} \sqrt{X} + O(X^{3/2})$ for small X , corroborating the anticipated parabolic contour near the crack tip.

To determine $\mathcal{U}(x)$, we introduce the dimensionless velocity $\mathcal{V} = \sqrt{2\pi} \lambda V \tau / L$. In the limit $y \rightarrow \pm 0$, Eq. (9) yields

$$\mathcal{U}(x) = \frac{2\varepsilon L}{\pi} \left[\arctan\left(\sqrt{e^X - 1}\right) - \left(1 - \frac{1}{\lambda}\right) H_{\mathcal{V}}(X) \right], \quad (16)$$

where

$$\begin{aligned} H_{\mathcal{V}}(X) &\equiv \frac{1}{2} \int_0^X \frac{e^{-(X-\Xi)/\mathcal{V}}}{\sqrt{e^\Xi - 1}} d\Xi \\ &= e^{-X/\mathcal{V}} \sqrt{e^X - 1} {}_2F_1\left(\frac{1}{2}, 1 - \frac{1}{\mathcal{V}}; \frac{3}{2}; 1 - e^X\right). \end{aligned} \quad (17)$$

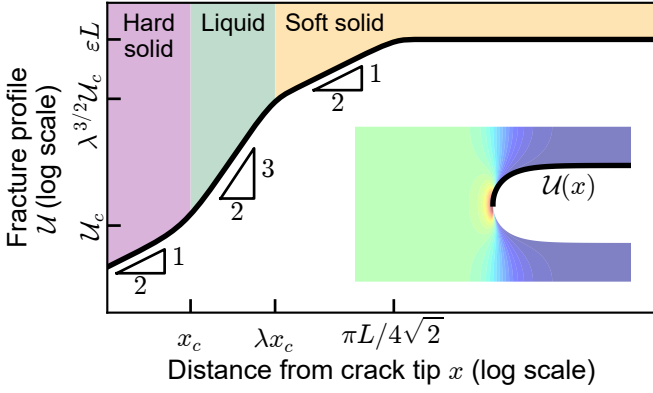


FIG. 3. Distinct regions within the fracture profile $\mathcal{U}(x)$ given by Eq. (16) in a log-log scale. Each region is characterized by a power-law exponent (1/2, 3/2, or 1/2) that evolves with the distance x from the crack tip. The ticks on the horizontal axis indicate the critical distances, x_c , λx_c , and $\pi L/4\sqrt{2}$, whereas the ticks on the vertical axis indicate the intersection points of respective asymptotic power laws, \mathcal{U}_c , $\lambda^{3/2}\mathcal{U}_c$ and εL . The condition $\lambda x_c < \pi L/4\sqrt{2}$ is necessary for the distinct manifestation of these power-law exponents. Inset shows the fracture profile $\mathcal{U}(x)$ in a linear scale; colors correspond to strain, as in Fig. 1.

Here, ${}_2F_1(a, b; c; z)$ is Gauss' hypergeometric function [31].

Based on the analytical expressions provided in the theorem, Fig. 2 shows the fracture profile $\mathcal{U}(x)$ and strain field $\mathcal{E}_{yy}(x, y)$ for slow [(a) $\mathcal{V} = 10^{-2}$] and fast [(b) $\mathcal{V} = 1$] crack propagations at $\lambda = 10^3$. To visualize the analytical solution accurately without losing precision through catastrophic cancellation, we utilized an arbitrary-precision library [32]. The fracture profile exhibits a parabolic contour at lower \mathcal{V} , transitioning to a sharper contour as \mathcal{V} increases.

Origin of crack-tip sharpening and viscoelastic trumpet. — To elucidate the origin of the crack-tip sharpening as \mathcal{V} increases, we examine the power-law behavior of the fracture profile $\mathcal{U}(x)$. We expand the expressions occurring in Eq. (16) in powers of X as

$$\arctan(\sqrt{e^X - 1}) = \sqrt{X} - \frac{X^{3/2}}{12} + O(X^{5/2}), \quad (18)$$

$$H_{\mathcal{V}}(X) = \sqrt{X} - \frac{(\mathcal{V} + 8)X^{3/2}}{12\mathcal{V}} + O(X^{5/2}). \quad (19)$$

These expansions yield the asymptotic behavior of $\mathcal{U}(x)$:

$$\mathcal{U}(x) \approx \frac{2\varepsilon L}{\pi} \begin{cases} \frac{1}{\lambda} \sqrt{X} & \text{for } 0 < X < X_c \\ \frac{2(\lambda - 1)}{3\lambda\mathcal{V}} X^{3/2} & \text{for } X_c < X < \lambda X_c \\ \sqrt{X} & \text{for } \lambda X_c < X < \frac{\pi^2}{4}, \end{cases} \quad (20)$$

where $X_c \equiv 3\mathcal{V}/2(\lambda - 1)$ and λX_c delineate the crossover points among these regions. For simplicity, in Eq. (20)

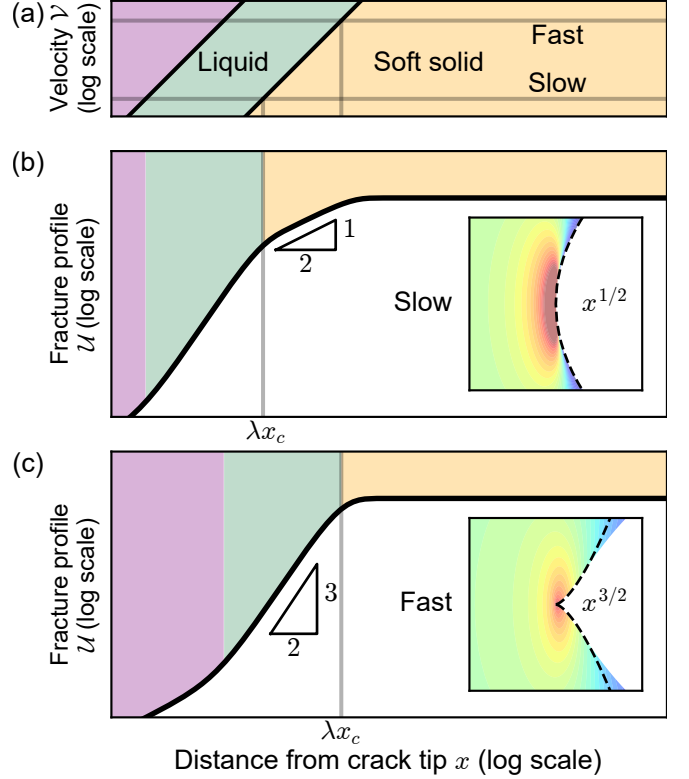


FIG. 4. Dependence of fracture profile on crack-propagation velocity V . (a) States of the viscoelastic solid on the crack surface as a function of the distance x from the crack tip, varying with V . Gray horizontal lines correspond to the fast and slow crack propagation cases shown in (b) and (c). Gray vertical lines indicate λx_c in (b) and (c). (b–c) Fracture profile \mathcal{U} during slow ($\mathcal{V} = 10^{-2}$) and fast ($\mathcal{V} = 1$) crack propagation. At low V , a smaller λx_c leads to dominance of the 1/2 power-law region, resulting in a parabolic profile at the crack tip. By contrast, at high V (c), a larger λx_c extends the 3/2 power-law region, resulting in a sharper profile at the crack tip.

and throughout this Letter, we assume $\lambda X_c < \pi^2/4$, which corresponds to $\mathcal{V} < \pi^2(1 - \lambda^{-1})/6$. Here, $\pi^2/4$ gives the threshold beyond which the sheet is fully relaxed (i.e., $\mathcal{U}(x) \approx \varepsilon L$ for $X > \pi^2/4$). Figure 3 shows $\mathcal{U}(x)$, revealing distinct power-law exponents for each region in Eq. (20): 1/2 near the crack tip, 3/2 beyond X_c up to λX_c , and 1/2 again beyond λX_c as $H_{\mathcal{V}}(X)$ becomes negligible. Note that because x is proportional to X , the exponents are the same regardless of the variable (x or X) used in the expansion.

Equation (20) is consistent with the viscoelastic trumpet, which is based on the assumption that $\lambda \gg 1$. Not only are the same exponents—1/2, 3/2, and 1/2—predicted in the viscoelastic trumpet [21, 22, 25, 33] but the crossover points delineating each region of the fracture profile, $x_c \equiv X_c L/\sqrt{2}\pi = 3\lambda V\tau/[2(\lambda - 1)] \approx 3V\tau/2$ and $\lambda x_c \approx 3\lambda V\tau/2$ for $\lambda \gg 1$, are also consistent with those of the viscoelastic trumpet ($V\tau$ and $\lambda V\tau$, respectively). Thus, our analysis elucidates the crack-tip dynamics in the linear viscoelastic regime and integrates the

viscoelastic trumpet with traditional fracture mechanics. Beyond identifying power-law exponents, Eq. (20) also provides the power-law prefactors within each region and the crossovers between them.

Figure 4(a) shows the state of the viscoelastic solid on the crack surface as a function of the distance x from the crack tip, varying with the crack-propagation velocity V . The black solid lines $x_c = 3\lambda V\tau/[2(\lambda - 1)]$ and $\lambda x_c = 3\lambda^2 V\tau/[2(\lambda - 1)]$ indicate the crossover points between the soft-solid, liquid, and hard-solid states. Both the soft and hard solids exhibit power-law exponents of $1/2$, yielding parabolic fracture profiles, whereas the liquid exhibits a power-law exponent of $3/2$, yielding a sharp profile. At lower V [Fig. 4(b)], the dominance of the $1/2$ power-law exponent and the small magnitudes of λx_c result in almost parabolic profiles. By contrast, at higher V [Fig. 4(c)], the increasing λx_c expands the liquid region, characterized by the prevailing $3/2$ power-law exponent. (Note that the scale in the figure is logarithmic.) This progressively sharpens the fracture profile.

Conclusion.— We have derived an analytical expression for the fracture profile [Eq. (16)] during steady-state crack propagation in viscoelastic solids, utilizing

the standard linear-solid model to describe viscoelasticity. The generality of the method used in this study is noteworthy, as it can be applied to a broad range of viscoelastic materials. Our solution identifies three distinct regions within the fracture profile [Eq. (20) and Fig. 3], each distinguished by characteristic power-law exponents that confirm the scaling theory in de Gennes' viscoelastic trumpet [21, 22]. Our findings not only validate the anticipated scaling behavior but also determine the power-law prefactors and the crossover points between these regions. This bridges a crucial gap in viscoelastic fracture mechanics, establishing a theoretical connection between the tip-sharpness and propagation velocity of a crack [Fig. 4]. By emphasizing the crucial role of viscoelastic effects, our research should facilitate the development of tough polymer materials by controlling crack-tip processes.

ACKNOWLEDGMENTS

This work was supported by JST PRESTO Grant Number JPMJPR1997, the establishment of university fellowships towards the creation of science technology innovation Grant Number JPMJFS2125, and JSPS KAKENHI Grant Number JP22H01187.

-
- [1] W. G. Knauss, A review of fracture in viscoelastic materials, *Int. J. Fract.* **196**, 99 (2015).
 - [2] C. Creton and M. Ciccotti, Fracture and adhesion of soft materials: a review, *Rep. Prog. Phys.* **79**, 046601 (2016).
 - [3] R. Long, C.-Y. Hui, J. P. Gong, and E. Bouchbinder, The fracture of highly deformable soft materials: A tale of two length scales, *Annu. Rev. Condens. Matter Phys.* **12**, 71 (2021).
 - [4] A. Kadir and A. G. Thomas, Tear Behavior of Rubbers Over a Wide Range of Rates, *Rubber Chem. Technol.* **54**, 15 (1981).
 - [5] K. Tsunoda, J. J. C. Busfield, C. K. L. Davies, and A. G. Thomas, Effect of materials variables on the tear behaviour of a non-crystallising elastomer, *J. Mater. Sci.* **35**, 5187 (2000).
 - [6] G. Carbone and B. N. J. Persson, Hot cracks in rubber: Origin of the giant toughness of rubberlike materials, *Phys. Rev. Lett.* **95**, 114301 (2005).
 - [7] Y. Morishita, K. Tsunoda, and K. Urayama, Velocity transition in the crack growth dynamics of filled elastomers: Contributions of nonlinear viscoelasticity, *Phys. Rev. E* **93**, 043001 (2016).
 - [8] N. Sakumichi and K. Okumura, Exactly solvable model for a velocity jump observed in crack propagation in viscoelastic solids, *Sci. Rep.* **7**, 8065 (2017).
 - [9] A. Kubo and Y. Umeno, Velocity mode transition of dynamic crack propagation in hyperviscoelastic materials: A continuum model study, *Sci. Rep.* **7**, 42305 (2017).
 - [10] A. Kubo, N. Sakumichi, Y. Morishita, K. Okumura, K. Tsunoda, K. Urayama, and Y. Umeno, Dynamic glass transition dramatically accelerates crack propagation in rubberlike solids, *Phys. Rev. Mater.* **5**, 073608 (2021).
 - [11] J. Murai, T. Nakajima, T. Matsuda, K. Tsunoda, T. Nonoyama, T. Kurokawa, and J. P. Gong, Tough double network elastomers reinforced by the amorphous cellulose network, *Polymer* **178**, 121686 (2019).
 - [12] C. Liu, H. Kadono, H. Yokoyama, K. Mayumi, and K. Ito, Crack propagation resistance of slide-ring gels, *Polymer* **181**, 121782 (2019).
 - [13] L. B. Freund, *Dynamic Fracture Mechanics* (Cambridge University Press, 1998).
 - [14] Y. Morishita, K. Tsunoda, and K. Urayama, Crack-tip shape in the crack-growth rate transition of filled elastomers, *Polymer* **108**, 230 (2017).
 - [15] T.-T. Mai, K. Okuno, K. Tsunoda, and K. Urayama, Crack-tip strain field in supershear crack of elastomers, *ACS Macro Lett.* **9**, 762 (2020).
 - [16] A. Livne, E. Bouchbinder, and J. Fineberg, Breakdown of linear elastic fracture mechanics near the tip of a rapid crack, *Phys. Rev. Lett.* **101**, 264301 (2008).
 - [17] E. Bouchbinder, A. Livne, and J. Fineberg, Weakly nonlinear theory of dynamic fracture, *Phys. Rev. Lett.* **101**, 264302 (2008).
 - [18] A. Livne, E. Bouchbinder, I. Svetlizky, and J. Fineberg, The near-tip fields of fast cracks, *Science* **327**, 1359 (2010).
 - [19] C.-H. Chen, E. Bouchbinder, and A. Karma, Instability in dynamic fracture and the failure of the classical theory of cracks, *Nat. Phys.* **13**, 1186 (2017).
 - [20] M. Wang, S. Shi, and J. Fineberg, Tensile cracks can shatter classical speed limits, *Science* **381**, 415 (2023).
 - [21] P. G. de Gennes, Soft adhesives, *Langmuir* **12**, 4497 (1996).
 - [22] P. G. de Gennes, *Soft Interfaces: The 1994 Dirac Memo-*

- rial Lecture* (Cambridge University Press, 1997).
- [23] B. N. J. Persson and E. A. Brener, Crack propagation in viscoelastic solids, *Phys. Rev. E* **71**, 036123 (2005).
- [24] B. N. J. Persson, O. Albohr, G. Heinrich, and H. Ueba, Crack propagation in rubber-like materials, *J. Phys.: Condens. Matter* **17**, R1071 (2005).
- [25] F. Saulnier, T. Ondarçuhu, A. Aradian, and E. Raphaël, Adhesion between a viscoelastic material and a solid surface, *Macromolecules* **37**, 1067 (2004).
- [26] H. Tabuteau, S. Mora, M. Ciccotti, C.-Y. Hui, and C. Ligoure, Propagation of a brittle fracture in a viscoelastic fluid, *Soft Matter* **7**, 9474 (2011).
- [27] W. G. Knauss, Stresses in an Infinite Strip Containing a Semi-Infinite Crack, *J. Appl. Mech.* **33**, 356 (1966).
- [28] M. Barber, J. Donley, and J. S. Langer, Steady-state propagation of a crack in a viscoelastic strip, *Phys. Rev. A* **40**, 366 (1989).
- [29] K. Okumura and P.-G. de Gennes, Why is nacre strong? elastic theory and fracture mechanics for biocomposites with stratified structures, *Eur. Phys. J. E* **4**, 121 (2001).
- [30] C. Zener, *Elasticity and Anelasticity of Metals* (University of Chicago Press, Chicago, 1948).
- [31] M. Abramowitz and I. Stegun, *Handbook of Mathematical Functions: With Formulas, Graphs, and Mathematical Tables*, Applied mathematics series (Dover Publications, 1965).
- [32] The mpmath development team, *mpmath: a Python library for arbitrary-precision floating-point arithmetic (version 1.3.0)* (2023), <http://mpmath.org/>.
- [33] C.-Y. Hui, B. Zhu, and R. Long, Steady state crack growth in viscoelastic solids: A comparative study, *J. Mech. Phys. Solids* **159**, 104748 (2022).